

# **Intercomparison of stratospheric HNO<sub>3</sub> measurements over Antarctica: Ground-based Millimeter-wave versus UARS /MLS Version 5 retrievals**

Giovanni Muscari<sup>1,3</sup>, Michelle L. Santee<sup>2</sup>, and Robert L. de Zafra<sup>1</sup>

<sup>1</sup>Institute for Terrestrial and Planetary Atmospheres, State University of New York, Stony Brook

<sup>2</sup>Jet Propulsion Laboratory, California Institute of Technology, Pasadena

<sup>3</sup> Now at Dipartimento di Fisica, Università degli studi di Roma "La Sapienza", Roma, Italy

Revised, Submitted to Journal of Geophysical Research, May 17, 2002

**Abstract.** We present the first intercomparison between the two most comprehensive records of gas-phase  $\text{HNO}_3$  profiles in the Antarctic stratosphere, covering the greater part of 1993 and 1995. We compare measurements by the Stony Brook Ground-Based Millimeter-wave Spectrometer (GBMS) at the South Pole with Version 5  $\text{HNO}_3$  data from the Microwave Limb Sounder (MLS) aboard the Upper Atmospheric Research Satellite. Trajectory tracing was used to select MLS measurements in the  $70^\circ$ - $80^\circ\text{S}$  latitude band that sampled air observed by the GBMS during passage over the Pole. When temperatures were near the  $\text{HNO}_3$  condensation range, additional screening was performed to select MLS measurements that sampled air parcels within 1.5 K of the temperature they experienced over the Pole. Quantitative comparisons are given at 7 different potential temperature levels spanning the range  $\sim 19$ - $30$  km. Agreement between the data sets is quite good between 465 and 655 K ( $\sim 20$ - $25$  km) during a large fraction of the year. Agreement is best during winter and spring, when seasonally averaged differences are generally within 1 ppbv below  $\sim 25$  km. At higher altitudes, and during summer and fall, the agreement becomes worse, and GBMS measurements can exceed MLS values by more than 3 ppbv. We provide evidence that differences occurring in the lower stratosphere during fall are due to lack of co-location between the two data sets during a period of strong poleward gradients in  $\text{HNO}_3$ . Remaining discrepancies between GBMS and MLS V5  $\text{HNO}_3$  measurements are thought to be due to instrumental or retrieval biases.

## 1. Introduction

Recent publications have reviewed in considerable detail the morphology of the HNO<sub>3</sub> seasonal cycle in the Antarctic stratosphere, describing its importance for Polar Stratospheric Cloud (PSC) particle formation and for determining the severity of springtime ozone loss [*de Zafra et al.*, 1997; *Santee et al.*, 1998, 1999; *McDonald et al.*, 2000; *Tabazadeh et al.*, 2000]. These studies have been based on independently derived data from separate ground- or satellite-based instruments which have not been compared yet with respect to HNO<sub>3</sub> retrievals. This study compares for the first time the two longest and most comprehensive records of gas-phase HNO<sub>3</sub> vertical profiles available in the Antarctic. One set of vertical profiles was retrieved by the Ground-Based Millimeter-wave Spectrometer (GBMS) at the South Pole, and the other set consists of the recently-released Upper Atmosphere Research Satellite (UARS) Microwave Limb Sounder Version 5 (MLS V5) retrievals. We stress here that although both the GBMS and MLS instruments measure pressure-broadened molecular rotation lines in emission, they observe different transitions and employ different observing geometries and deconvolution methods to retrieve mixing ratio profiles from the pressure-broadened line shapes.

While the present study was in progress, it was discovered that emissions from the HNO<sub>3</sub> v<sub>9</sub> and v<sub>7</sub> excited vibrational states, which were omitted from the V5 retrieval algorithm, are significant in the spectral region in which MLS HNO<sub>3</sub> is retrieved. Neglecting the contributions from these lines caused the retrieved MLS V5 values to significantly overestimate HNO<sub>3</sub> abundances at some levels in the stratosphere. An

empirical correction to the MLS V5 HNO<sub>3</sub> data set has recently been derived and is described in detail in *Livesey et al.* [“The UARS Microwave Limb Sounder Version 5 dataset: Theory, characterization, and validation”, manuscript submitted, March 2002]. The correction is a linear, strongly temperature-dependent scaling of the original V5 HNO<sub>3</sub> values. For example, the correction leads to reductions in the reported V5 HNO<sub>3</sub> mixing ratios of about 4-8% at 100 hPa, 10-20% at 32 hPa, and 25-35% at 10 hPa, depending on the latitude and season. In the comparisons here we use the corrected MLS HNO<sub>3</sub> data.

Our comparison encompasses two periods: from April 1993 to January 1994 and from March to November 1995. These periods are determined by data availability and temporal overlap, which will be discussed in the next section.

## 2. Measurements

Vertical profiles of gas-phase HNO<sub>3</sub> (throughout this paper, unless we explicitly state otherwise, all references to HNO<sub>3</sub> will be to gas-phase HNO<sub>3</sub>) were retrieved during 1993, 1995 [*McDonald et al.*, 2000], and 1999 by the GBMS set up at the Amundsen-Scott Base, located at the geographic South Pole. We have chosen to compare only data from 1993 and 1995 because MLS data at Antarctic latitudes are sparse or absent during most of 1999. Ground-based measurements were carried out twice a week, on average, although (especially in 1995) there were some periods of instrumental inactivity or malfunction, with no data available. A detailed description of the GBMS experimental apparatus and observational technique is given by *de Zafra* [1995], while the accuracy of the constrained matrix inversion procedure [*Twomey*, 1977] used to deconvolve HNO<sub>3</sub>

spectral lines is discussed in *de Zafra et al.* [1997]. GBMS measurements are integrated over about 6 hours, in nearly all cases roughly centered around 12:00, and have an altitude range of 16-50 km ( $\sim 75$ -0.35 hPa). Although the instantaneous field of view of the GBMS is about 10 km in width (defined as the half-width of a gaussian antenna response) at  $\sim 23$  km of altitude, the integration time of each measurement means that the GBMS samples an air stream typically 200-300 km in length, as air moves over the Pole. The vertical resolution of profiles is determined by the full width at half-maximum (FWHM) of the averaging kernels used in the inversion algorithm, and increases with altitude from  $\sim 5$  km to  $\sim 8$  km. Tests have shown, however, that the GBMS retrievals typically locate the altitude of the maximum mixing ratio in a resolved HNO<sub>3</sub> layer to within  $\sim 2$  km (for a detailed discussion, see [*de Zafra et al.*, 1997, Appendix]). The overall uncertainty in the retrieved mixing ratios (including both systematic and random errors) varies with altitude and time and is bounded approximately between 16% and 22%. GBMS data are retrieved as a function of pressure, but are published and archived as a function of altitude every 2 km, using locally measured meteorological data to translate from pressure to altitude.

MLS acquired HNO<sub>3</sub> profiles from September 1991 to August 2001, although problems with the instrument scan system as well as the spacecraft solar array and batteries caused a drastic reduction (or the total lack) of observations during several periods of time (for example: from October 1994 to July 1995, and after June 1997). MLS measurements have a horizontal resolution of  $\sim 400 \times 400$  km and extend from 80° on one side of the equator to 34° on the other, alternating 10 times per year between viewing northern and southern high latitudes (see *Santee et al.* [1999] and references

therein for further details). A detailed description of the MLS V5 data processing algorithm and validation of the V5 data products is given by *Livesey et al.* [manuscript submitted, March 2002]; information about the quality of the V5 retrievals is also available from the MLS web site (<http://mls.jpl.nasa.gov>). MLS V5 retrievals are obtained from inversion of spectral radiances using the optimal estimation method [*Rodgers, 1976, 2000*]. We again emphasize that the HNO<sub>3</sub> retrievals used in the present paper have been corrected for the influence of v7 and v9 excited vibrational states which had been omitted from the original V5 processing (see preceding section for details).

In V5, geophysical parameters are reported on all 6 standard UARS pressure levels per decade of pressure (twice the vertical resolution of the previous MLS data sets). The true vertical resolution of the MLS V5 HNO<sub>3</sub> data set has not doubled, however, since some vertical smoothing has been applied for retrieval stability [*Livesey et al.*, manuscript submitted, March 2002]. The vertical resolution of the MLS V5 HNO<sub>3</sub> profiles is defined by the FWHM of the rows of the averaging kernel matrix produced by the retrieval algorithm and increases with altitude from ~ 5 km to ~ 10.5 km. The single profile precision varies with altitude as well, and typical values are between 1 and 1.5 ppbv over the range from 100 hPa to 4.6 hPa (~ 15-35 km), above which the reliability of the HNO<sub>3</sub> data has not been established (other MLS V5 products have a much larger vertical range). The estimated accuracy of the MLS V5 has not yet been rigorously quantified because a sufficient number of comparisons with correlative data sets have not been made. The MLS V5 HNO<sub>3</sub> uncertainties adopted in this study include only the random noise contribution and thus represent a lower bound on the total uncertainty in

the data. In this intercomparison we used only measurements that passed all the quality control checks for both data sets.

In the current study, air parcels have been traced on quasi-isentropic trajectories. To provide a common altitude measure, we have chosen to interpolate all data to a set of seven potential temperature ( $\theta$ ) levels close to the six standard UARS pressure levels used for MLS V5 HNO<sub>3</sub> retrievals, plus one additional level to allow a better characterization of the peak of the HNO<sub>3</sub> distribution. The chosen levels are 465, 520, 585, 620, 655, 740, and 960 K. It should be noted that the HNO<sub>3</sub> values obtained at these levels are not all independent since neither the MLS nor the GBMS data have enough vertical resolution to separate out each of these surfaces. (The vertical resolution of both instruments expressed in potential temperature is  $\sim 100$  K at  $\theta = 465$  K and approximately 350 K for GBMS and 450 K for MLS at  $\theta = 960$  K. As pointed out in Section 2, however, GBMS retrievals proved to have an accuracy of  $\sim 2$  km or  $\sim 60$  K in locating the altitude of the HNO<sub>3</sub> mr peak.) To interpolate both data sets onto the chosen  $\theta$  levels, we use the daily global assimilated pressure and temperature data from the U.K. Meteorological Office [*Swinbank and O'Neill, 1994*] interpolated to the location of interest. This interpolation to theta surfaces can in principle alter the relationship of retrievals between the two datasets, but our tests show these effects to be small relative to the larger retrieval uncertainties.

### **3. Quasi-isentropic trajectories**

Since GBMS measurements are taken at 90°S, and MLS reaches a southernmost latitude of about 80°, the two sets of data are never co-located. To compensate for this,

we used the trajectory mapping technique, first proposed by *Morris et al.* [1995], to connect air parcels passing over the Pole with locations of MLS measurements. We employed the quasi-isentropic Goddard Space Flight Center (GSFC) trajectory model [*Schoeberl et al.*, 1995], which advects air parcels backward or forward in time with respect to an initial position using horizontal wind velocity fields and diabatic heating rates (proportional to vertical transport). For each run we initiated trajectory traces at 8 locations surrounding the Pole (at 4 cardinal points separated 90 degrees in longitude and by offsets of 0.5 and 1.0 degrees in latitude from the Pole) at noon of any day when GBMS data are available. (This generally matches the mean time of day when GBMS data were taken.) After running the individual trajectories, all the parameters (position, temperature, etc.) of the 8 parcels were averaged together at each time step along their trajectories, and the resultant averaged trajectory was used to select MLS retrievals to compare with GBMS data (see next section for details). In  $< 10\%$  of the traces, one of the 8 parcels would begin to deviate substantially (by more than  $40^\circ$  in longitude or  $2.5^\circ$  in latitude) from the averaged trajectory position and was therefore dropped from the averaging process. We always have at least 6 parcels available to compute an average position. We ran 5-day trajectories both backward and forward in time, at each of the seven  $\theta$  surfaces encompassed in the comparison and listed in the previous section. As an example, Figure 1 shows 5-day backward and 5-day forward trajectories starting over the South Pole on June 3, 1993, at 520 K. Note that both backward and forward traces may lead to intersections with MLS data within the maximum allotted time span.

#### **4. Intercomparison**

Our intercomparison is based on a varying number of days of GBMS and MLS V5 data, depending on the potential temperature level and the period of time considered. Between April 1993 and January 1994 there are about 30 to 34 days of GBMS data (out of a total of 63 days of GBMS measurements) that can be compared to MLS V5 data in the fashion illustrated below. Between April and November 1995 there are fewer data available for both data sets, and the number of coincidences ranges from 10 to 16, depending on the  $\theta$  level.

Several conditions have to be met to obtain one correlation point. First of all, MLS must have collected data in the south-viewing mode (therefore reaching  $80^{\circ}\text{S}$ ) on at least one day out of the 5 days preceding or following a GBMS day of measurement. (The more days of MLS data available for this 10-day period, the higher the chance of obtaining a correlation point.) The second step in the data selection process is performed using the GSFC trajectory model. As mentioned in Section 3, we average together, at each time step, all the parameters related to the 8 parcels run backward or forward for 5 days from the South Pole, obtaining an “averaged” trajectory. We look at the averaged trajectory data and find the locations of the parcel at noon for all the days that the parcel spent between  $70^{\circ}\text{S}$  and  $80^{\circ}\text{S}$ . We choose  $70^{\circ}\text{S}$  as the northern boundary to obtain and average together a sufficient number of MLS V5 measurements, while still minimizing the distance between the GBMS profiles observed at the Pole and the MLS V5 measurements selected. The day numbers and the parcel’s location associated with each day are recorded, and for each of these days we consider MLS measurements (if any are available) within a box of  $\pm 10^{\circ}$  longitude (approximately  $\pm 287$  km) and  $\pm 2.5^{\circ}$  latitude (approximately  $\pm 278$  km) around the location where the parcel is found during a specific

day. (Sensitivity studies that led to this choice of box size are illustrated in the Appendix.) In fact, because of the finite MLS footprint, these measurements can be representative of an area slightly larger than the one mentioned above.

Daily MLS observations belonging to a specified box are first interpolated onto the  $\theta$  level where the parcel is located (which may be somewhat different from the South Pole  $\theta$  starting values listed above), and then averaged together using a  $\cos^2(d)$  weighting function depending on their distance “d” from the center of the box (“d” is normalized to have  $\cos^2(d) = 0$  at the edges of the box). At this stage of the process, we have a spatially-averaged value of MLS  $\text{HNO}_3$  mr for each day when the following two conditions coexist: 1) MLS V5 data are available, and 2) the air parcel is between  $70^\circ\text{S}$  and  $80^\circ\text{S}$ . Next, we average together over time those values that belong to air parcels that passed over our initiating points around the Pole (see Section 3) on the same day “N”, either on a forward or a backward trajectory. For this temporal average, we use a  $\cos^2(t)$  algorithm, where t is the time in days between a spatially-averaged MLS day of measurement and day N (normalized to  $\cos^2(t) = 0$  when  $t = \pm 7$ ). This spatially- and temporally-averaged MLS  $\text{HNO}_3$  mr value (from now on “MLS V5 AVE”) is then compared with the GBMS value measured at the Pole on day N. We repeat this process for each of the seven  $\theta$  levels mentioned above and for each of the GBMS days of data available.

During winter periods, if temperatures are around the PSC formation thresholds, temperature gradients along trajectories can cause condensation of  $\text{HNO}_3$  on PSC particles or its release back to the gas phase during the time between  $\text{HNO}_3$  measurements by MLS and by GBMS. Therefore, for winter comparisons at all levels except 960 K (where temperatures are always above PSC thresholds), we carry out an

additional selection of MLS data: the temporal average of daily, spatially-averaged MLS V5 HNO<sub>3</sub> mr values along a trajectory is performed using only those daily values obtained when the air parcel's temperature at noon is within 1.5 K of the temperature experienced by the parcel over the Pole.

The acceptance window for MLS data of  $\pm 1.5$  K from the temperature at the South Pole was chosen as the smallest value that could be imposed while still maintaining a sufficient number of MLS V5 AVE data points. This value is smaller than the temperature uncertainty of  $\pm 3$  K adopted in this study following the recommendation of *Manney et al.* [1996] and *McDonald et al.* [2000] (see Section 5). Because of this uncertainty in temperature, which is critical when temperatures are close to threshold values for PSC particle formation, and because the HNO<sub>3</sub> condensation/evaporation process is highly non-linear with temperature, our temperature screening will not completely eliminate cases in which the same air parcel contains a different HNO<sub>3</sub> concentration when sampled by MLS and by GBMS. Tests (not shown) have demonstrated, however, that winter results are only slightly sensitive to variations of the acceptance window within the temperature uncertainty of  $\pm 3$  K.

To illustrate the usefulness of this temperature screening, in Figure 2 we have plotted the time series of temperature, latitude position, and MLS V5 HNO<sub>3</sub> mr along the forward and backward trajectories starting at the South Pole on June 3, 1993, at the four levels where we observed the largest temporal gradients in MLS V5 HNO<sub>3</sub> mr. We have chosen June 3 because it is one of the few cases where a large number of MLS V5 days of data (10) could be averaged together to calculate an MLS V5 AVE point. The 10 individual MLS measurements provide the good temporal resolution needed to show how

HNO<sub>3</sub> mr variations follow temperature trends. During most of the 10 days of MLS V5 data considered (five days before reaching the Pole and five after), temperatures are warmer than over the Pole by up to 7-8 K, and values lie in the range considered critical for PSC particle formation. MLS V5 HNO<sub>3</sub> mr trends match temperature trends well, underlining the rapidity of the HNO<sub>3</sub> depletion/restoration mechanism and its dependence on temperature. At each of the 4 altitude levels shown in Figure 2, MLS V5 AVE (open circle) agrees more closely with the value obtained by GBMS (open square) than does the weighted average (star) of all the MLS V5 daily values within  $\pm 5$  days of the parcel's passage over the Pole (solid circles).

We have also considered the question of whether, at the highest two levels in this comparison, photolysis occurring along trajectories over a 3-5 day period of changing solar exposure at certain times of year could alter HNO<sub>3</sub> mixing ratios significantly between GBMS and MLS observations. Various studies [e.g., *Brasseur and Solomon*, 1984; *Morris et al.*, 1997] have in fact shown that the photochemical lifetime of HNO<sub>3</sub> is already in excess of 10 days at 740 K (~27 km) and increases very rapidly with decreasing altitude. Tests using a chemical box model derived from the Stony Brook-St. Petersburg two-dimensional model [*Smyshlyaev et al.*, 1998] additionally verify negligible change in HNO<sub>3</sub> mr along the trajectories that we employ for levels 740 and 960 K.

For each GBMS day of data, we do not always obtain a selection of MLS measurements at all the  $\theta$  surfaces considered. This happens because trajectory paths may enter the 70°S-80°S latitude range at some altitudes and not at others or, because of different air speeds at different altitudes, they may enter it during different days. Thus,

even though on one day there may be MLS V5 data available at all levels, on the next day there might not be.

We turn next to consideration of the horizontal and temporal resolution of MLS V5 averages. To allow the gathering of a statistically significant number of MLS V5 data points, MLS data are averaged daily from within a box  $\pm 10^\circ$  longitude by  $\pm 2.5^\circ$  latitude (an area of about 320,000 km<sup>2</sup>). The horizontal resolution is also further diminished by the 24-hour resolution of our intercomparison: GBMS data (typically integrated over  $\sim 6$  consecutive hours spanning mid-day), MLS V5 spatial averages, and the air parcel positions are all downgraded to daily 12:00 GMT values for our comparisons. Therefore, the distance between the instantaneous position of an air parcel (e.g., near midnight) and the location of an MLS V5 vertical profile associated with the parcel (e.g., near the edge of the averaging box traced around the parcel's position at noon) could be as much as 1000 km (half length of the averaging box plus the distance advanced in the opposite direction by the parcel in 12 hours). These necessary spatial and temporal averaging processes diminish the spatial resolution and therefore the accuracy of the intercomparison. It is likely that MLS measurements of HNO<sub>3</sub> concentration in the air parcel that GBMS observed a few days earlier or later at 90°S are averaged together with HNO<sub>3</sub> concentrations belonging to air parcels that never reached 90°S. Sensitivity tests described in the Appendix and shown in Plate A support this argument. Results employing MLS V5 averages over larger areas show larger discrepancies between the two data sets. Such discrepancies diminish when going from zonal averages to averaging boxes and then decrease further with the decrease of the dimensions of the averaging box (see Appendix, panel 4 of Plate A), providing evidence that it would be misleading to

compare GBMS data from the South Pole to simple averages of MLS V5 inner-vortex data (represented, for example, by the 75°-80°S zonal averages shown in Plate A). Our final choices of temporal and spatial coincidence criteria used to compare the two data sets are driven by the need of both reasonable time and space resolutions and a sufficient number of coincidences to make data comparisons statistically significant. We found that a further restriction of either the temporal or spatial resolution would not significantly change our results (several of the tests relevant to this issue are illustrated in the Appendix). The size of the averaging box we chose is comparable to the intrinsic horizontal resolutions of MLS and GBMS data.

A trajectory technique similar to the one developed here was used by *Morris et al.* [2000] to work out four different data comparisons. *Danilin et al.* [2002] also adopted a conceptually similar approach to prove the effectiveness of trajectory-based data selection in validating multi-platform measurements. Although the trajectory calculations themselves are subject to uncertainties, both *Morris et al.* [2000] and *Danilin et al.* [2002] concluded that the use of backward and forward trajectories is a reliable tool for estimating measurement accuracy and precision and is suitable for data validation studies. In fact, they find that trajectory techniques can perform even better than traditional approaches that use only co-located data: the use of trajectories increases the number of coincidences between two sets of measurements without significantly increasing the uncertainty of the comparisons.

## 5. Results

In Plate 1(a-g) nitric acid time series for the year 1993 are shown, with blue squares representing GBMS data (all available days) and red circles representing MLS V5 AVE values, corrected as described in Section 1 for the influence of previously omitted vibrational state transitions. We plot all available GBMS days of data to show their trend during periods when there are no matching MLS data. Error bars on GBMS daily mixing ratios represent the overall uncertainty (see Section 2). The error estimates on the MLS V5 AVE mixing ratios are obtained by propagating the error of the individual profiles. When averaging a number “n” of MLS V5 data points, the error on the average MLS V5 value is taken to be the average of the n errors divided by  $(n)^{1/2}$ . For the temperature profiles used in the interpolation of  $\text{HNO}_3$  data on  $\theta$  surfaces, we adopted an uncertainty of  $\pm 3$  K [Manney *et al.*, 1996; McDonald *et al.*, 2000: Section 3.2]. Such an uncertainty propagates to a minimum error  $\Delta\theta \sim 7$  K at  $\theta = 465$  K and a maximum error  $\Delta\theta \sim 14$  K at  $\theta = 960$  K. These uncertainties on the  $\theta$  levels are incorporated in the MLS V5 AVE uncertainties through the error propagation method. Results from 1995 data are similar to those obtained in 1993; as an example 1995 results at 465 K are shown in Plate 1h.

Plate 1 shows that GBMS measurements and MLS V5 AVE generally agree well at lower levels during concurrent periods of observation, displaying  $\text{HNO}_3$  seasonal variations that are similar in both timing and magnitude, although a few exceptions exist and will be discussed later. At 740 and 960 K,  $\text{HNO}_3$  mr values from GBMS are consistently larger than MLS V5 AVE. To quantify the level of agreement and the systematic differences between the two data sets, the 1993 and 1995 GBMS and MLS V5 AVE data have each been averaged with equal weight into 5 periods (from now on called pseudo-seasons), determined by seasons and  $\text{HNO}_3$  annual evolution. Although we show

all available GBMS data in Plate 1, GBMS data used in the seasonal binning include only days with a corresponding MLS V5 AVE day of data, to insure that the two data sets are averaged over the same temporal windows within any pseudo-season boundaries. Temporal boundaries of these pseudo-seasons are indicated in Plates 1(a-h) with vertical dashed lines. The pseudo-seasons are formally defined as: Fall (F; from day 71 to day 145), Early Winter (EW; from day 146 to day 210), Late Winter (LW; from day 211 to day 265), Spring (Sp; from day 266 to day 355), and Summer (Su; from day 356 to day 375 (365+10)). The division of winter into two periods is dictated by a substantial change in HNO<sub>3</sub> trends at most altitudes of interest between day 190 and day 210.

The early winter and late winter periods are the most statistically robust, since they rely on a large number of coincidences (mostly in 1993). The uncertainty of the pseudo-seasonal averages is computed as the maximum probable error,  $\delta(\text{mr}) = \Sigma_i \delta(\text{mr}_i)/N$ , where N is the total number of observations averaged together, and the  $\delta(\text{mr})_i$  are the error estimates inherent in the individual mixing ratios shown in Plate 1.

In Figure 3, we present both the absolute differences  $D_{\text{abs}} = \text{GBMSseas} - \text{MLSseas}$  in ppbv (black bars) and the relative differences

$$D_{\%} = 100 \times \frac{\text{GBMSseas} - \text{MLSseas}}{1/2 \times (\text{MLSseas} + \text{GBMSseas})}$$

(gray bars) between the pseudo-seasonal averages described above, at each chosen altitude level. The GBMS and MLS V5 AVE pseudo-seasonal averages are indicated by GBMSseas and MLSseas, respectively, and include only days when both data sets are available. The error bars are computed on the assumption that the MLS and GBMS data and associated errors are completely uncorrelated: for the absolute differences

$$\delta D_{\text{abs}} = \sqrt{(\delta \text{GBMSseas})^2 + (\delta \text{MLSseas})^2},$$

and for the relative uncertainties,

$$\delta D_{\%} = D_{\%} \times \left( \frac{\delta D_{\text{abs}}}{\text{GBMSseas} - \text{MLSseas}} + \frac{\delta D_{\text{abs}}}{\text{GBMSseas} + \text{MLSseas}} \right),$$

where  $\delta \text{GBMSseas}$  and  $\delta \text{MLSseas}$  are the uncertainties of the pseudo-seasonal averages.

Absolute differences are  $\leq 2$  ppbv for 24 of the 35 comparisons (69% of the time) and are  $> 3$  ppbv in only 5 cases, mostly at 960 K or during the summer period. The estimated error bar for absolute differences overlaps zero 77% of the time, and GBMS seasonal averages are larger than those from the corrected MLS V5 57% of the time. Where mixing ratios are small, typically at 960 K and in LW at levels 465 through 620 K, percentage differences can be very large and are a poor indicator of the agreement between the two data sets. (For this reason we have omitted the relative difference for the late winter period at 465 K, since the MLS value is very close to zero.) With the exception of the upper two levels, absolute differences in Figure 3 generally show very good agreement between GBMS and MLS data in early winter and spring, while the largest discrepancies occur in fall and summer. At levels 740 and 960 K, a systematic offset is evident in 9 cases out of 10 (see Figure 3). The MLS  $\text{HNO}_3$  mr values at these altitudes appear to be quite homogeneous in the  $70^\circ$ - $80^\circ$  latitude band (see Appendix, panel 3 of Plate A), which should minimize random discrepancies caused by the lack of co-location between the two data sets. We believe instead that an instrumental or retrieval bias exists at these levels between MLS and GBMS. In particular, MLS V5  $\text{HNO}_3$  data also exhibit a low bias above 750 K in comparison with measurements by the Improved Limb Atmospheric Spectrometer (ILAS) [Danilin *et al.*, 2002], suggesting that, at the

upper two levels studied here, values obtained by GBMS are likely to be more reliable than those of MLS V5.

We discuss intercomparisons within various pseudo-seasons in further detail in the following sub-sections.

### 5.1. Fall

During fall, shortly after polar sunset ( $\sim$  day 80), with temperatures still above 200 K in the 15 to 30 km altitude region, nitrogen species are heterogeneously converted to  $\text{HNO}_3$  on background aerosols [e.g., *Solomon et al.*, 1992], causing the increase in mr that can be seen in Plate 1 peaking between days 110 and 140 (see also Plate 1 of *McDonald et al.* [2000]). A switch to the north-looking observing mode of MLS interrupts data coverage at high southern latitudes just as  $\text{HNO}_3$  over the Pole reaches its concentration peak before condensation begins.

As emphasized in Figure 3, averaged values of  $\text{HNO}_3$  mixing ratio retrieved by GBMS over the Pole during this pseudo-season are larger than those obtained by MLS at  $70^\circ$ - $80^\circ\text{S}$  at all levels except 465 K. Differences are between 1 and 3 ppbv or between 15% and 20% at all levels except 960 K, where the discrepancy increases due to the GBMS outlier on day 113, 1993. We believe that the observed difference between the two data sets at lower altitudes is in large part caused by the heterogeneous conversion process mentioned above, combined with the spatial resolution limits of our comparison method discussed in Section 4. The heterogeneous  $\text{HNO}_3$  formation is dependent on  $\text{N}_2\text{O}_5$  concentrations and therefore on the length of nighttime experienced by an air mass. Air at 23 km ( $\sim$  585 K) is still exposed to  $\sim$  9 hours of sunlight at  $70^\circ\text{S}$  on day 115, while on the

same day it is subjected to only  $\sim 4.5$  hours of sunlight at  $80^\circ\text{S}$ . A latitudinal gradient in  $\text{HNO}_3$  mr is thus established in the lower stratosphere and contributes to the differences observed during fall at levels 520 K through 655 K. This gradient can be seen in panels 1 and 2 of Plate A (Appendix). Levels 740 K and 960 K, at  $\sim 27$  and 31 km, respectively, are not characterized by a large latitudinal gradient in MLS retrievals however (see panel 3 of Plate A), but still display a substantial positive bias in GBMS relative to MLS retrievals in the very limited time of overlap before MLS switches to northward observing at about day 115. As pointed out earlier, this positive bias, although variable in magnitude, is in fact present throughout the year at levels 740 and 960 K, with the only exception being the summer average at 960 K.

To further investigate the larger amounts of  $\text{HNO}_3$  found by GBMS with respect to MLS during fall, we looked at another set of  $\text{HNO}_3$  measurements carried out during the same period. In a comparison study between MLS V5 and the UARS Cryogenic Limb Array Etalon Spectrometer (CLAES) (Version 9), the latter shows even smaller values of  $\text{HNO}_3$  than MLS V5 (by as much as 3 ppbv) during the austral fall from 465 K to 620 K, while the two data sets agree within 1 ppbv at higher altitudes [*Livesey et al.*, manuscript submitted, March 2002].

We then address the question of whether the larger  $\text{HNO}_3$  mr values measured by GBMS during fall are inconsistent with measurements of total reactive nitrogen ( $\text{NO}_y$ ). In the polar darkness, conversion of NO and  $\text{NO}_2$  to  $\text{N}_2\text{O}_5$  takes place rapidly, followed by hydrolysis of  $\text{N}_2\text{O}_5$  to  $\text{HNO}_3$  on sulfate aerosols [e.g., *Garcia and Solomon*, 1994; *Santee et al.*, 1999; *de Zafra and Smyshlyaev*, 2001]. We thus expect  $\text{HNO}_3$  to represent almost 100% of  $\text{NO}_y$  in the polar stratosphere during late fall and winter at altitudes up to  $\sim 23$

km [Garcia and Solomon, 1994; Schneider, et al., 1999; Michelsen et al., 1999]. In Figure 4 we have plotted the  $\text{NO}_y\text{-N}_2\text{O}$  correlation curve obtained at midlatitudes ( $44^\circ\text{-}55^\circ\text{S}$ ) by ATMOS/ATLAS-2 in April 1993 [e.g., Michelsen et al., 1998], together with the  $\text{HNO}_3\text{-N}_2\text{O}$  correlation obtained using GBMS profiles at  $90^\circ\text{S}$  (for GBMS  $\text{N}_2\text{O}$  retrievals see Crewell et al. [1995]) from April 15, 1993 (day 105), which is during our fall pseudo-season and more than 3 weeks after sunset at the South Pole. Figure 4 shows that the GBMS  $\text{HNO}_3$  measurements from the Pole are in good agreement with ATMOS midlatitude  $\text{NO}_y$  values from the lowest altitudes sampled by GBMS ( $\sim 15$  km,  $\theta \sim 410$  K,  $\text{N}_2\text{O} \sim 238$  ppbv) up to the  $\text{HNO}_3$  mr peak ( $\sim 23$  km,  $\theta \sim 585$  K,  $\text{N}_2\text{O} \sim 85$  ppbv). At higher altitudes ( $\text{N}_2\text{O} < 80$  ppbv in Figure 4), GBMS  $\text{HNO}_3$  is well below ATMOS total  $\text{NO}_y$ : here the partition of reactive nitrogen compounds shifts towards  $\text{NO}_2$  and  $\text{NO}$ , as atmospheric pressure and ozone concentration decrease, and  $\text{HNO}_3$  mr decreases sharply with altitude [Brasseur and Solomon, 1984]. We conclude from the evidence in Figure 4 that the GBMS measurements at the Pole are not inconsistent at any altitude with total  $\text{NO}_y$  measured by ATMOS at  $44^\circ\text{-}55^\circ\text{S}$ . Unfortunately, no fall measurements of total  $\text{NO}_y$  concurrent with GBMS or MLS V5 data from the southern polar region are available to further validate the  $\text{HNO}_3$  peak values measured in fall by GBMS.

## 5.2. Early Winter

The Early Winter lower stratosphere is characterized by a further temperature decrease within the vortex and a subsequent condensation of  $\text{HNO}_3$  on sulfate aerosols and PSC particles. In this period GBMS and MLS agree very well at levels from 465 K to 620 K, showing absolute differences within 1 ppbv, and are still in fairly good agreement

at 655 K and 960 K, where GBMS is biased high with respect to MLS by 1.2 and 1.5 ppbv, respectively. Relative differences are within 10% at levels from 520 K to 655 K, but increase at 465 and 960 K, where mixing ratios are small. Level 740 K shows instead a large disagreement of more than 3 ppbv, which is consistent with results obtained for this level during all pseudo-seasons.

### 5.3. Late Winter

By the beginning of the Late Winter pseudo-season, most lower stratospheric  $\text{HNO}_3$  is incorporated into PSC particles and very little is left in the gas phase. In contrast to this scenario in the lower stratosphere, large concentrations of reactive nitrogen ( $\text{NO}_y$ ) move down into the upper and middle stratosphere during polar winter [e.g., *Russell et al.*, 1984; *Siskind et al.*, 2000, and references therein], and its partitioning shifts towards  $\text{HNO}_3$  while descending to lower altitudes [e.g., *Kawa et al.*, 1995; *de Zafra and Smyshlyaev*, 2001]. Thus, in the stratosphere at altitudes where temperature remains above the PSC condensation temperature, the  $\text{HNO}_3$  mr is observed to increase through descent and conversion of odd nitrogen ( $\text{NO}_x$ ) from the upper and mid stratosphere [*de Zafra et al.*, 1997; *McDonald et al.*, 2000].

As observed in most seasons, we also find in Late Winter that differences between GBMS and MLS V5 data at 740 and 960 K are larger than those at lower levels. This persistent offset at the upper two levels is discussed in the Results section. At lower levels (465 through 655K), absolute differences in this season are not significantly different from other seasons, but percentage differences tend to be large because absolute values are quite small. Considering this period in more detail, Plate 1 shows that at levels

585 and 620 K (and perhaps less clearly as low as 520 K) the trend of MLS V5 AVE data points is different from that of GBMS data: by the end of EW, GBMS HNO<sub>3</sub> mixing ratios reach a minimum at or near 0 ppbv, remain there until day 220-230, and then increase with time until they match MLS V5 AVE values just after day 240. In contrast, MLS V5 AVE data seem to bottom out at 3-5 ppbv towards the end of EW and resume this range of values when MLS turns southward again on day 220.

Meteorological data show that temperatures remained consistently below 190 K in the altitude range between 16 km ( $\theta \sim 385$  K) to 26 km ( $\theta \sim 680$  K) over the Pole from day 165 through day 230, and in much of this vertical range and time span, temperatures were consistently below 185 K. This is well below the temperature range for HNO<sub>3</sub> condensation onto PSCs [e.g., *Santee et al.*, 1998, and references therein]. After about day 230, temperatures steadily increased at level 585 K, while remaining between 180 K and 185 K at level 520 K until after day 250. We thus believe that GBMS observations, showing essentially no HNO<sub>3</sub> at lower altitudes during the transition from EW to LW, are consistent with physical temperatures and the established condensation processes of PSCs, as is the increase in HNO<sub>3</sub> mr that characterizes GBMS data later in LW (see Plate 1).

Since MLS V5 data were selected using the temperature screening procedure described in Section 4, all the air parcels involved in calculation of MLS V5 AVE points plotted in Plate 1 encountered temperatures similar to those measured over the Pole during GBMS observations. We would therefore expect MLS V5 HNO<sub>3</sub> mr values to follow GBMS data down to or near zero at  $\sim 520$  to 620 K. We believe that the disagreement between MLS and GBMS in this season primarily arises from

nonlinearities with respect to temperature in the MLS retrieval system, which can cause retrieved values to be too large in the Antarctic winter polar vortex [*Livesey et al.*, manuscript submitted, March 2002].

#### 5.4. Spring

In spring, daylight returns after the winter darkness and temperatures inside the vortex rise. By day 280 over the Pole, only a thin stratospheric layer between 14 – 20 km ( $\theta \sim 360 - 520$  K) is below 195 K, and this disappears by day 300. Antarctic nitric acid at lower levels gradually increases due to a combination of evaporation of remnant PSCs, continued descent from higher levels where  $\text{HNO}_3$  formed in winter, and advection from regions outside the weakened vortex. When the vortex breaks up towards the end of the season, the intrusion at high latitudes of air previously confined outside the vortex causes a large variability in polar stratospheric  $\text{HNO}_3$  mr.

Both data sets show the gradual recovery of nitric acid during the Spring period (Plate 1), with a close match between many MLS V5 and GBMS data points and agreement of seasonal averages to within 1 ppbv from 465 to 655 K and 2 ppbv at levels 740 and 960 K (Figure 3). We note that this period exhibits a much larger variation in GBMS values at most levels than any other period, though MLS data do not show this. Concurrent GBMS observations of  $\text{N}_2\text{O}$  published by *Crewell et al.* [1995] show strong signs of vortex break up and intrusion of air with high concentrations of  $\text{N}_2\text{O}$  at the same time GBMS  $\text{HNO}_3$  mr profiles become quite variable. Since MLS V5 measurements have been spatially averaged in this study (see Section 4), they may fail to depict the localized daily variations present in the GBMS  $\text{HNO}_3$  mr profiles.

## 5.5. Summer

The comparison for the summer season relies only on 1993 data, since no coincidences were found in summer 1995. Only 3 or 4 data points (depending on the altitude) are available and the statistics are therefore not very robust. The agreement between the two data sets is to within 1 ppbv at levels 465, 520, and 960 K, while GBMS values are larger than MLS V5 averages by 2 to 4.5 ppbv at all other levels (Figure 3). This offset was not reduced by any additional selection constraints on MLS V5 profiles, such as the use of 2-day instead of 5-day air trajectories, and no latitudinal gradient is indicated during summer in Plate A. We therefore consider the discrepancy a real bias between the two data sets and not a consequence of their lack of co-location, though reiterating that the number of coincidences found during this season is small.

## 6. Summary

We have made a comparison of the most recently released MLS V5 profiles for HNO<sub>3</sub> between 70°-80°S, after correction for the effect of previously omitted vibrational state transitions, with those retrieved by a ground-based instrument at the South Pole. The comparison extends over two almost complete annual cycles, providing information on differences between HNO<sub>3</sub> measured by the two instruments under a wide variety of stratospheric conditions and nitric acid abundances. Air parcel trajectories, supplemented in winter by temperature screening, have been employed to further select MLS V5 profiles for the comparison. Sensitivity studies presented in the Appendix are used to justify the choices made in matching data with trajectories and to infer which

discrepancies between the two sets of measurements are probably due to latitudinal gradients in  $\text{HNO}_3$  mr and not to instrumental or retrieval biases.

The largest differences between GBMS and MLS V5  $\text{HNO}_3$  measurements are generally found in Fall and Summer at most levels. Differences are also large at the top two  $\theta$  levels studied in this work, 740 and 960 K, where nearly all GBMS values are larger than MLS V5 averages and absolute differences can exceed 3 ppbv, suggesting the possibility of a low bias in the MLS measurements at these levels. Such a low bias is also indicated in a recent comparison between MLS V5 and ILAS  $\text{HNO}_3$  measurements [Danilin *et al.*, 2002]. In the Fall season, a combination of  $\text{HNO}_3$  latitudinal gradients and the spatial resolution limits of our comparison method could explain a large part of the discrepancy between GBMS and MLS V5  $\text{HNO}_3$  mr values, while in Summer we have not found a plausible explanation for the differences observed. The agreement between the two data sets is generally quite good between 465 and 655 K, during the pseudo-seasons of Early Winter, Late Winter, and Spring, where absolute differences are within  $\pm 1.3$  ppbv, except for LW at 585 K, where the absolute difference increases to  $\sim 1.8$  ppbv (Figure 3). The LW differences below 655 K are driven by very small GBMS mr values. We note, however, that values near zero ppbv are consistent with known PSC condensation and temperature data, and suggest that larger MLS values retrieved for levels below 655 K during the winter period may be an artifact arising from nonlinearities with respect to temperature in the MLS retrieval system.

## Appendix: Sensitivity studies

To make sure that the MLS V5 AVE values obtained were not strongly dependent on arbitrary parameters such as the area encompassed by the box or the weighting functions applied, several sensitivity tests were run. One set of tests investigated the size of the region within which MLS V5 measurements are averaged together (eventually set to  $\pm 10^\circ$  longitude and  $\pm 2.5^\circ$  latitude, and called Box 1 in the text below). Plots in Plate A show clearly what the trends are when zonally averaged data are collected progressively further away from the Pole and illustrate how differences between the two data sets diminish when the trajectory technique is used instead of a simple zonal average. In particular, since during winter the  $75^\circ$ - $80^\circ$ S zonal averages are roughly equivalent to averages of inner-vortex MLS data, Plate A shows the improvement obtained using a trajectory tracing technique versus a comparison with daily averages of all the available MLS inner-vortex data. In fall, more  $\text{HNO}_3$  is heterogeneously produced on sulfate particles at the Pole than at equatorward polar locations sampled by MLS. In early winter, colder temperatures at the Pole increase the rate at which  $\text{HNO}_3$  is absorbed onto PSC particles, making the  $\text{HNO}_3$  depletion earlier and greater. Moreover, colder temperatures cause stronger denitrification at the Pole and therefore less  $\text{HNO}_3$  is recovered at the end of the winter period, as shown in the late winter and spring measurements. The time series shown in panels 1 and 2 of Plate A are representative of differences between MLS V5 data averages found at the four lower levels, while data from higher levels (Plate A shows only  $\theta = 960$  K in panel 3), which have little or no  $\text{HNO}_3$  depletion from condensation on PSCs, indicate smaller or negligible differences between the 3 MLS V5 time series.

We also ran tests to find what box size would give the best results (eventually called Box 1). We tested the following box sizes:  $\pm 5^\circ$  longitude by  $\pm 1.25^\circ$  latitude (Box 2),  $\pm 15^\circ$  longitude by  $\pm 3^\circ$  latitude (Box 3), and  $\pm 90^\circ$  longitude by  $\pm 5^\circ$  latitude (Box 4). For this test, data extracted from these boxes were spatially averaged without using any weighting function in order to maximize the importance of the box size parameter. Results are shown in Plate A, panel 4, for the 585 K level, which gives a good representation of results from all seven  $\theta$  levels. The figure shows the time series of GBMS data and that of MLS V5 AVE obtained with Boxes 2 and 4 (respectively the smallest and the largest considered). Results from Box 3 lie in between those for Box 2 and 4 and are not shown. Although Box 4 is extremely large, differences between results from Box 2 and 4 still tend to be small. However, in all pseudo-seasons except summer, biases can be discerned, and results obtained using Box 2 generally stay closer to GBMS data points than do the results from Box 4. Such  $\text{HNO}_3$  mr differences are the largest in early winter and the smallest in summer, matching the degree of inhomogeneity of Antarctic  $\text{HNO}_3$  shown by *Santee et al.* [1999] in their Plate 1. Therefore, during most pseudo-seasons, using Box 4 means averaging over air masses with very different physical and chemical properties. Although the Box 2 results seem to capture better the air masses that passed over the Pole, very few MLS V5 measurements can be found in such a small box, and the statistics obtained are not very robust. A larger box (Box 1) with a  $\cos^2(d)$  spatial weighting function obtains basically the same results as Box 2, but can rely on a larger number of MLS V5 measurements for each box. Furthermore, the size of Box 1 is comparable to the horizontal resolution of both MLS and GBMS;

therefore, choosing a much smaller size for the averaging box would not improve the accuracy of the comparison results.

Additional tests were conducted to study the sensitivity of the results to the spatial weighting function used.  $\text{Cos}(d)$  and linear functions were applied and their results showed no substantial differences compared to those obtained with the  $\text{cos}^2(d)$  function. Results differed (slightly) only when no weight at all was applied to the spatial average.

**Acknowledgments.** This research was supported by the National Science Foundation under Grants No. OPP-9117813 and No. OPP-9705667, and by NASA under Grant No. NAG 54071. The work at the Jet Propulsion Laboratory was done under contract with NASA. We thank Mark Schoeberl and his collaborators at the Goddard Space Flight Center for their trajectory model and Wei-Wu Tan for running it for us. We thank Bill Read for his efforts in correcting the MLS V5 HNO<sub>3</sub> data set. We also wish to thank Curt Trimble and Richard Chamberlin for the GBMS observations made in 1993 and 1995, respectively, and Randy Kawa and Nathaniel Livesey for helpful suggestions and discussions relating to some of the material in this manuscript.

## References

- Brasseur G., and S. Solomon, *Aeronomy of the middle atmosphere*, D. Reidel, Dordrecht, Holland, 1984.
- Crewell, S., D. Cheng, R. L. de Zafra, and C. Trimble, Millimeter wave spectroscopic measurements over the South Pole, 1. A study of stratospheric dynamics using N<sub>2</sub>O observations, *J. Geophys. Res.*, 100, 20,839-20,844, 1995.
- de Zafra, R. L., The ground-based measurements of stratospheric trace gases using quantitative millimeter wave emission spectroscopy, in “*Diagnostic tools in atmospheric physics*”, Proceedings of the international school of physics “Enrico Fermi”, pp. 23-54, Società Italiana di Fisica, Bologna, 1995.
- de Zafra, R. L., V. Chan, S. Crewell, C. Trimble, and J. M. Reeves, Millimeter wave spectroscopic measurements over the South Pole: 3. The behavior of stratospheric nitric acid through polar fall, winter, and spring, *J. Geophys. Res.*, 102, 1399-1410, 1997.
- Danilin, M. Y., M. K. W. Ko, L. Froidevaux, M. L. Santee, L. V. Lyjak, R. M. Bevilacqua, J. M. Zawodny, Y. Sasano, H. Irie, Y. Kondo, J. M. Russell III, C. J. Scott, and W. G. Read, Trajectory hunting as an effective technique to validate multi-platform measurements: Analysis of the MLS, HALOE, SAGE-II, ILAS, and POAM-II data in October-November 1996, *J. Geophys. Res.*, in press, 2002.
- de Zafra, R. L., and S. P. Smyshlyaev, On the formation of HNO<sub>3</sub> in the Antarctic mid-to-upper stratosphere in winter, *J. Geophys. Res.*, 106, 23,115-23,125, 2001.
- Garcia, R. R., and S. Solomon, A new numerical model of the middle atmosphere 2. Ozone and related species, *J. Geophys. Res.*, 99, 12,937-12,951, 1994.

- Kawa, S. R., J. B. Kumer, A. R. Douglass, A. E. Roche, S. E. Smith, F. W. Taylor, and D. J. Allen, Missing chemistry of reactive nitrogen in the upper stratospheric polar winter, *Geophys. Res. Lett.*, 22, 2629-2632, 1995.
- Manney, G. L., R. W. Zurek, A. O'Neill, and R. Swinbank, On the motion of air through the stratospheric polar vortex, *J. Atm. Sci.*, 51, 2973-2994, 1994.
- Manney, G. L., R. Swinbank, S. T. Massie, M. E. Gelman, A. J. Miller, R. Nagatani, A. O'Neill, and R. W. Zurek, Comparison of U.K. Meteorological Office and U.S. National Meteorological Center stratospheric analyses during northern and southern winter, *J. Geophys. Res.*, 101, 10,311-10,334, 1996.
- McDonald, M. K., R. L. de Zafra, and G. Muscari, Millimeter wave spectroscopic measurements over the South Pole: 5. Morphology and evolution of HNO<sub>3</sub> vertical distribution, 1993 versus 1995, *J. Geophys. Res.*, 105, 17,739-17,750, 2000.
- Michelsen, H.A., G.L. Manney, M.R. Gunson, and R. Zander, Correlations of stratospheric abundances of NO<sub>y</sub>, O<sub>3</sub>, N<sub>2</sub>O, and CH<sub>4</sub> derived from ATMOS measurements, *J. Geophys. Res.*, 103, 28,347-28,359, 1998.
- Michelsen, H.A., et al., Maintenance of high HCl/Cl<sub>y</sub> and NO<sub>x</sub>/NO<sub>y</sub> in the Antarctic vortex: A chemical signature of confinement during spring, *J. Geophys. Res.*, 104, 26,419-26,436, 1999.
- Morris, G. A., M. R. Schoeberl, L. C. Sparling, P. A. Newman, L. R. Lait, L. Elson, J. Waters, R. A. Suttie, A. Roche, J. Kumer, and J. M. Russell, III, Trajectory mapping and applications to data from the Upper Atmosphere Research Satellite, *J. Geophys. Res.*, 100, 16,491-16,505, 1995.

Morris, G. A., D. B. Considine, A. E. Dessler, S. R. Kawa, J. Kumer, J. Mergenthaler, A. Roche, and J. M. Russell III, Nitrogen partitioning in the middle stratosphere as observed by the Upper Atmospheric Research Satellite, *J. Geophys. Res.*, *102*, 8955-8965, 1997.

Morris, G. A., J. F. Gleason, J. Ziemke, and M. R. Schoeberl, Trajectory mapping: a tool for validation of trace gas observations, *J. Geophys. Res.*, *105*, 17,875-17,894, 2000.

Rodgers, C.D., Retrieval of atmospheric temperature and composition from remote measurement of thermal radiation, *Rev. Geophys.*, *14*, 609-624, 1976.

Rodgers, C.D., *Inverse methods for atmospheric sounding: theory and practice*, World Scientific, 2000.

Russell, J. M. III, S. Solomon, L. L. Gordley, E. E. Remsberg, and L. B. Callis, The variability of stratospheric and mesospheric NO<sub>2</sub> in the polar winter night observed by LIMS, *J. Geophys. Res.*, *89*, 7267-7275, 1984.

Santee, M. L., A. Tabazadeh, G. L. Manney, R. J. Salawitch, L. Froidevaux, W. G. Read, and J. W. Waters, UARS Microwave Limb Sounder HNO<sub>3</sub> observations: Implications for Antarctic polar stratospheric clouds, *J. Geophys. Res.*, *103*, 13,285-13,313, 1998.

Santee, M. L., G. L. Manney, L. Froidevaux, W. G. Read, and J. W. Waters, Six years of UARS Microwave Limb Sounder HNO<sub>3</sub> observations: Seasonal, interhemispheric, and interannual variations in the lower stratosphere, *J. Geophys. Res.*, *104*, 8225-8246, 1999.

- Schoeberl, M. R., and L. C. Sparling, Trajectory modeling, in "*Diagnostic tools in atmospheric physics*", Proceedings of the international school of physics "Enrico Fermi", pp. 289-305, IOS Press, Amsterdam, 1995.
- Schneider, J., et al., The temporal evolution of the ratio  $\text{HNO}_3/\text{NO}_y$  in the Arctic lower stratosphere from January to March 1997, *Geophys. Res. Lett.*, 26, 1125-1128, 1999.
- Siskind, D. E., G. E. Nedoluha, C. E. Randall, M. Fromm, J. M. Russell III, An assessment of Southern Hemisphere stratospheric  $\text{NO}_x$  enhancements due to transport from the upper atmosphere, *Geophys. Res. Lett.*, 27, 329-332, 2000.
- Smyshlyaev, S. P., V. Dvortsov, M. A. Geller, and V. Yudin, A two-dimensional model with input parameters from a general circulation model: ozone sensitivity to different formulations for the longitudinal temperature variation, *J. Geophys. Res.*, 103, 28,373-28,387, 1998.
- Solomon, S., and J. G. Keys, Seasonal variations in Antarctic  $\text{NO}_x$  chemistry, *J. Geophys. Res.*, 97, 7971-7978, 1992.
- Swinbank, R., and A. O'Neill, A stratosphere-troposphere data assimilation system, *Mon. Weather Rev.*, 122, 686-702, 1994.
- Tabazadeh, A., M. L. Santee, M. Y. Danilin, H. C. Pumphrey, P. A. Newman, P. J. Hamill, J. L. Mergenthaler, Quantifying denitrification and its effect on ozone recovery, *Science*, 288, 1407-1411, 2000.
- Twomey, S., Introduction to the mathematics of inversion in remote sensing and indirect measurements, in *Developments in Geomathematics*, vol. 3, Elsevier Sci., New York, 1977.

-----  
R. L. de Zafra, Department of Physics and Astronomy, State University of New York,  
Stony Brook, NY 11794-3800.

G. Muscari, Dipartimento di Fisica, Università degli studi di Roma "La Sapienza", P.le  
Aldo Moro 5, Roma, Italy (e-mail: muscari@g24ux.phys.uniroma1.it).

M. L. Santee, Jet Propulsion Laboratory, Mail Stop 183-701, 4800 Oak Grove Drive,  
Pasadena, CA 91109.

## CAPTIONS

**Figure 1.** 5-day backward and forward trajectories originating at the South Pole on June 3, 1993, at  $\theta = 520$  K. Triangles indicate the daily position of the 8 parcels at noon. Latitude circles are at  $60^{\circ}\text{S}$ ,  $70^{\circ}\text{S}$ , and  $80^{\circ}\text{S}$ .

**Plate 1(a-h).** Time series of GBMS data (blue squares) and MLS V5 AVE (red circles) for 1993 (all levels studied) and 1995 (only shown at  $\theta = 465$  K). GBMS error bars include both systematic and random error. MLS V5 AVE red error bars represent the MLS V5 random error propagated through the interpolation and averaging processes, while the gray error bars show the minimum and maximum MLS V5 values used in the computation of each MLS V5 AVE point. Vertical dashed lines mark the 5 pseudo-seasons defined in the text and specified in the top panels. The months of the year are indicated above the top panels by their initials.

**Figure 2.** Time series of temperature (solid thin line), latitude position (dashed thin line) and MLS V5 HNO<sub>3</sub> data (solid circles connected by thick dash-dotted lines) along the forward and backward trajectories ending at the South Pole on June 3, 1993. Central Y-axes show mixing ratio in ppbv. The GBMS value for June 3 is indicated in each panel with an open square. The weighted average of all selected MLS V5 daily values within  $\pm 5$  days of passage over the Pole (what in Fall, Spring, and Summer would be a MLS V5 AVE point) is shown in each panel with a star. The MLS V5 AVE point obtained averaging together only those MLS V5 daily values that passed temperature screening (see text) is indicated with an open circle. Note that MLS V5 AVE points (open circles) agree better with the GBMS measurements from June 3 (open squares) than do the weighted averages over  $\pm 5$  days (stars).

**Figure 3.** Absolute differences (GBMS – MLS) in mixing ratios (black bars, in ppbv, left hand ordinate) and relative differences (GBMS - MLS) / MLS x 100 (gray bars, right hand ordinate) for each pseudo-season in Plate 1. The computation of error bars is described in the text. We have omitted the relative difference for the LW period at 465 K, since the MLS value is very close to zero.

**Figure 4.** Correlations of NO<sub>y</sub>-N<sub>2</sub>O (thick solid line) from the ATMOS/ATLAS-2 mission and of HNO<sub>3</sub>-N<sub>2</sub>O (open circles) from GBMS data. ATMOS/ATLAS-2 data were collected in the 44°-55°S latitude band during the period April 8-16, 1993. Thin dashed lines show the range of uncertainty for the ATMOS correlation, given NO<sub>y</sub> and N<sub>2</sub>O mr accuracies of 15% and 5%, respectively [e.g., *Michelsen et al.*, 1998]. The

GBMS correlation was obtained at 90°S using HNO<sub>3</sub> and N<sub>2</sub>O mr profiles from April 15, 1993. The error bars represent the total uncertainties of HNO<sub>3</sub> (see text) and N<sub>2</sub>O [Crewell *et al.*, 1997].

**Plate A.** A sample of results from sensitivity studies. Panels 1, 2 and 3 show time series of GBMS data (blue squares), MLS V5 zonal averages in the 70°-75°S latitudinal band (green solid circles), MLS V5 zonal averages in the 75°-80°S latitudinal band (red solid circles), and MLS V5 AVE values (black solid circles) at three different  $\theta$  levels. Panel 4 shows results obtained using different box sizes for MLS V5 AVE averages. Results with Box 2 (the largest) are shown with green open circles, results with Box 4 (the smallest) are the red open circles, and GBMS time series is indicated with blue open squares. Vertical dashed lines mark the 5 pseudo-seasons defined in the text and specified in the top panels.

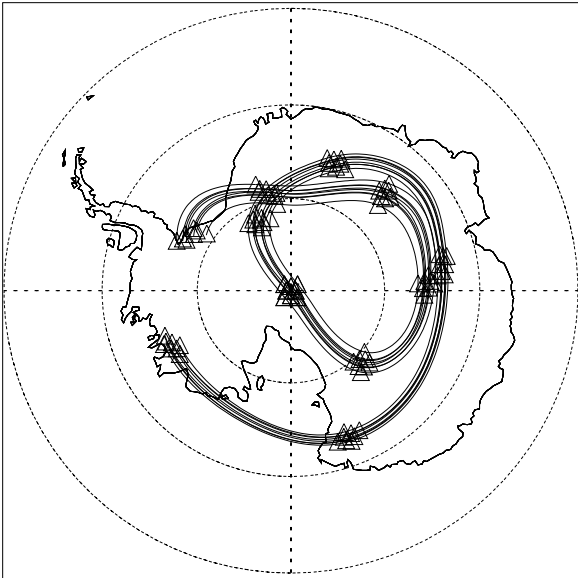


**Figure 1.**

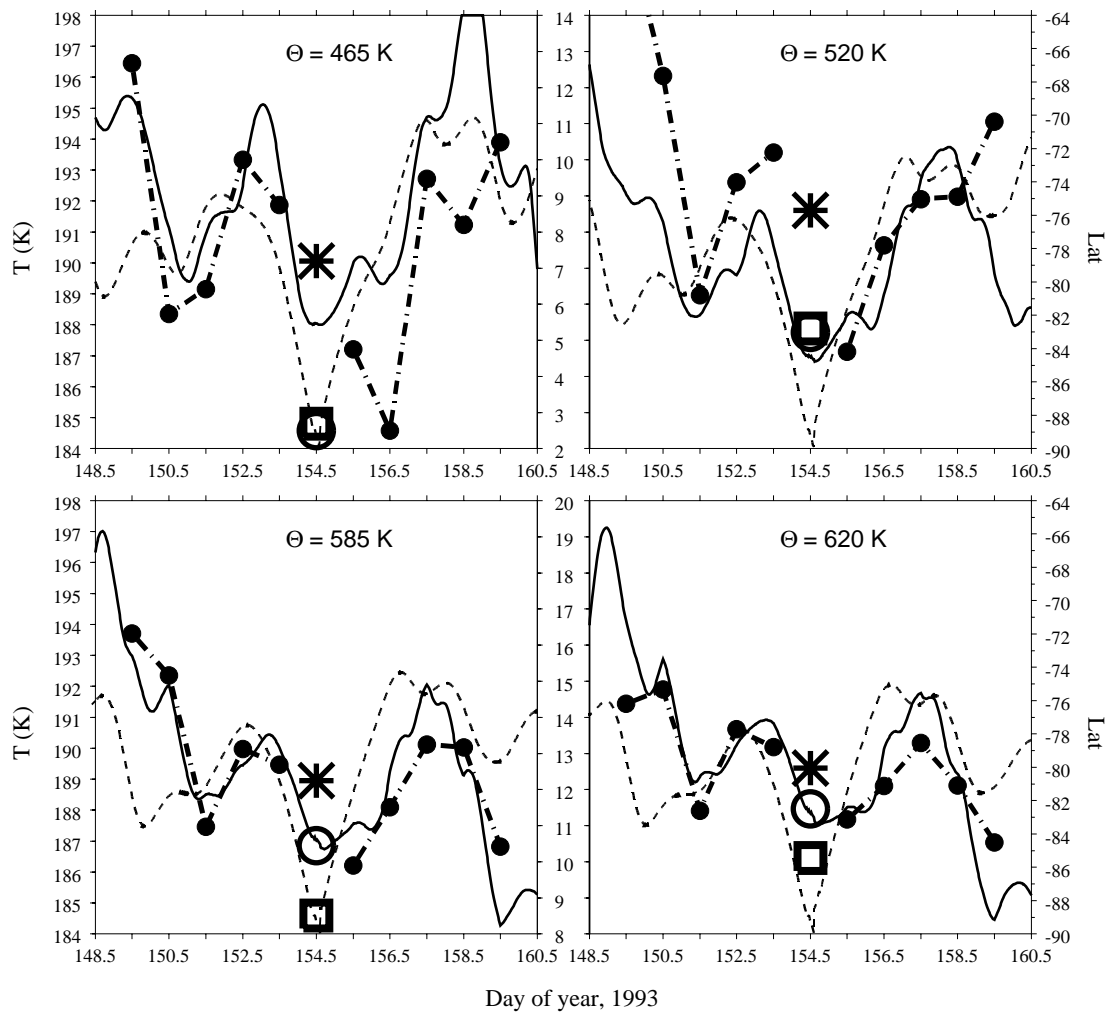


Figure 2.

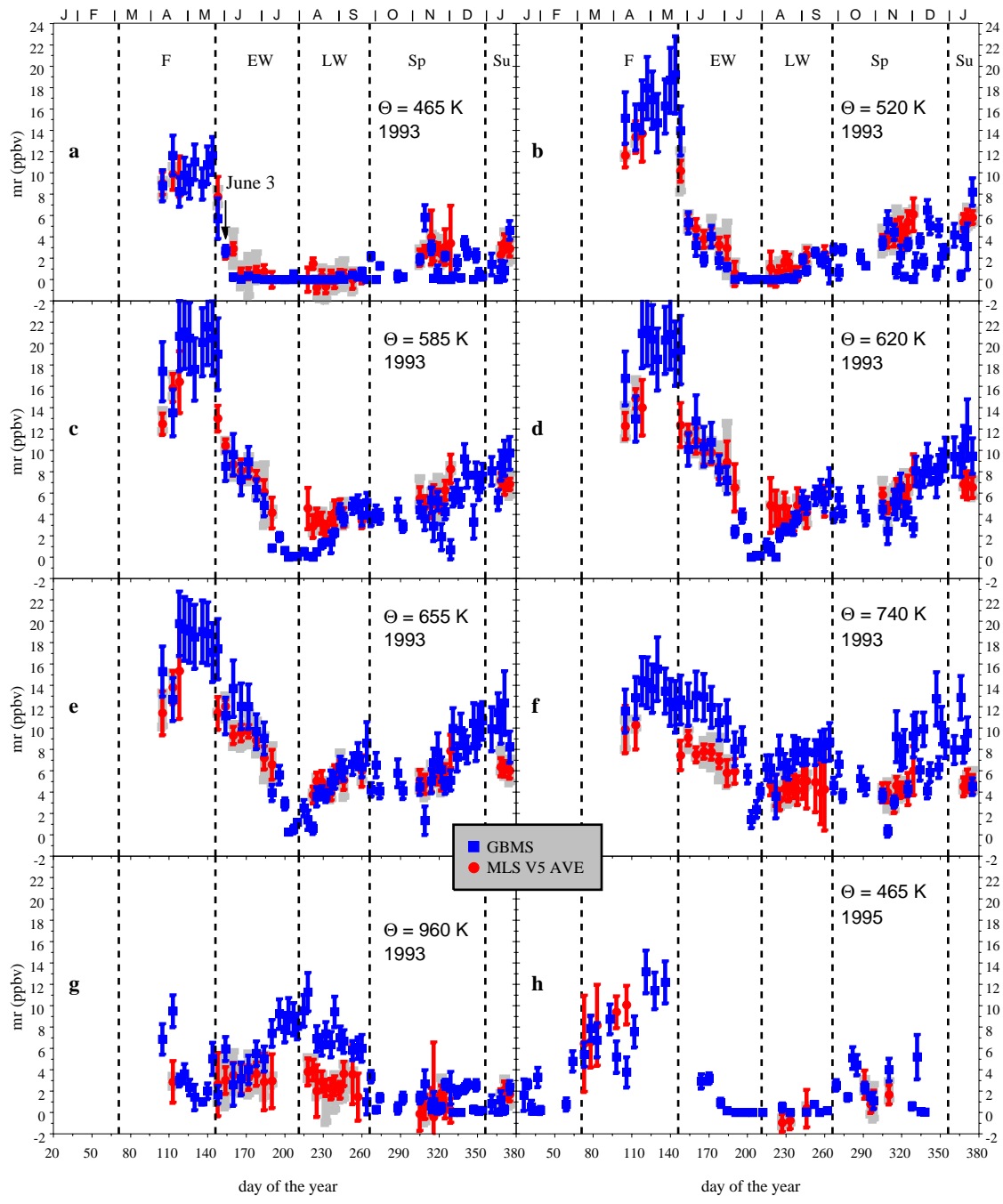


Plate 1.

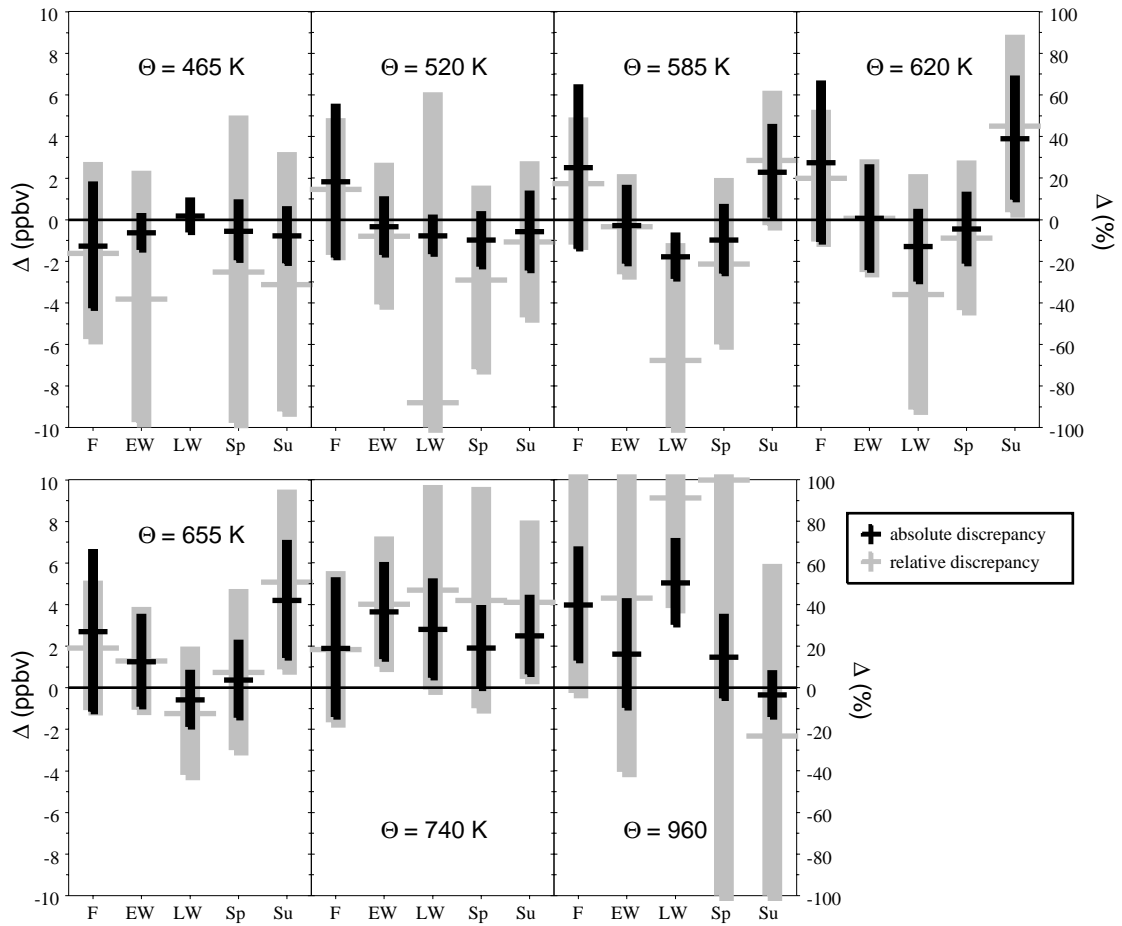


Figure 3.

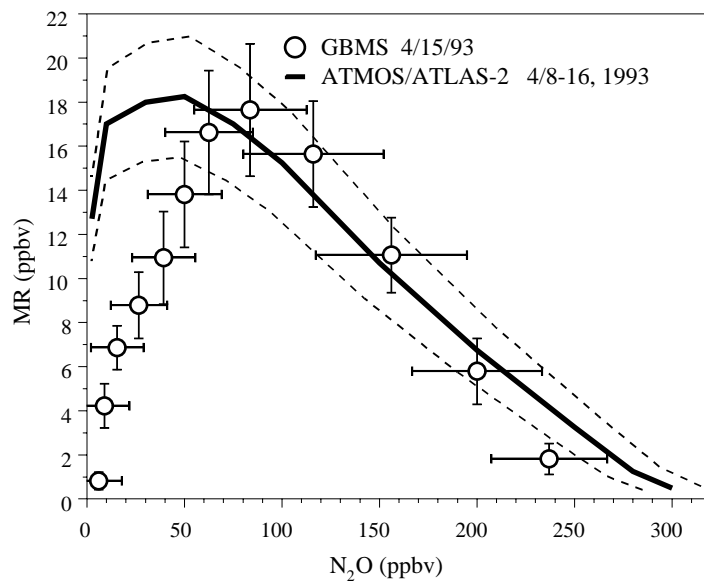


Figure 4.

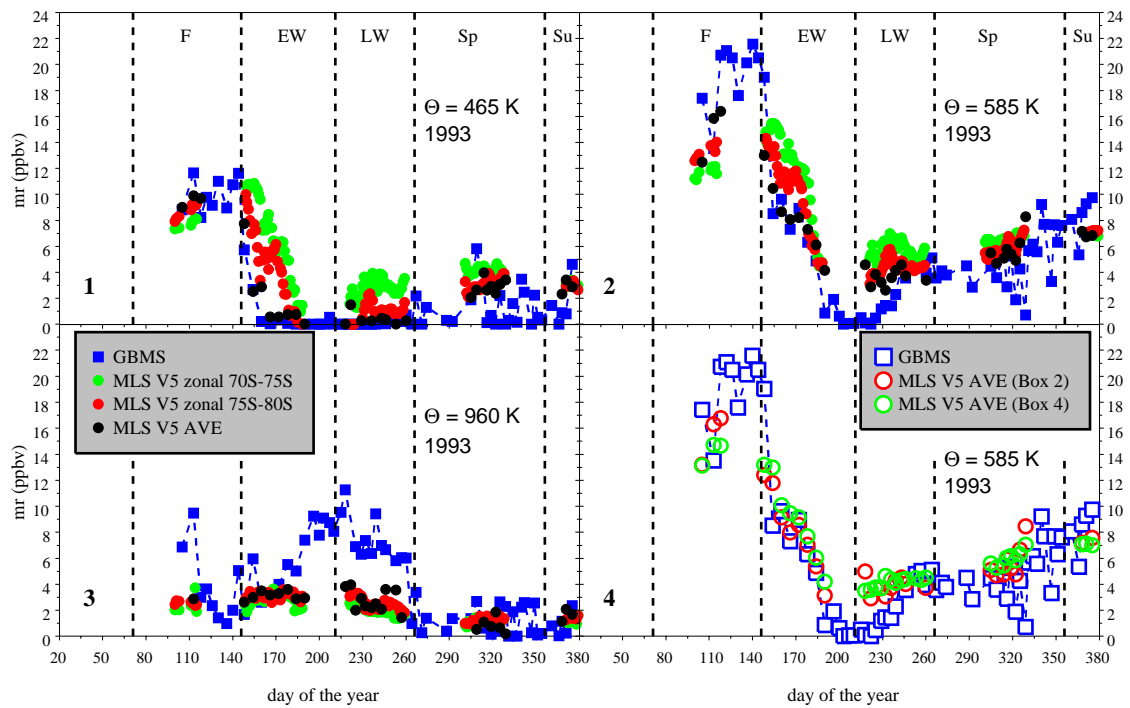


Plate A.